ADVANCED MATERIALS

www.advmat.de

3D Printing of Customized Li-Ion Batteries with Thick Electrodes

*Teng-Sing Wei, Bok Yeop Ahn, Julia Grotto, and Jennifer A. Lewis**

The growing demand for rechargeable lithium-ion batteries (LIBs) with higher capacity in customized geometries underscores the need for new battery materials, architectures, and assembly strategies. Here, the design, fabrication, and electrochemical performance of fully 3D printed LIBs composed of thick semisolid electrodes that exhibit high areal capacity are reported. Specifically, semisolid cathode and anode inks, as well as UV curable packaging and separator inks for direct writing of LIBs in arbitrary geometries are created. These fully 3D printed and packaged LIBs, which are encased between two glassy carbon current collectors, deliver an areal capacity of 4.45 mAh cm^{-2} at a current density of 0.14 mA cm^{-2}, which is equivalent to 17.3 Ah L^{-1}. The ability to produce high-performance LIBs in customized form factors opens new avenues for integrating batteries directly within 3D printed objects.

Rechargeable Li-ion batteries (LIBs) are widely used in applications ranging from portable electronics[1] to electric vehicles.[2] Commercial LIBs are limited to simple shapes (e.g., coin, cylinder, prismatic, and pouch cells), composed of thin electrodes (20–100 μm thick), and separated by a polymer or polymer–ceramic film that are repeated, stacked, and sandwiched between two current collecting (metal) foils.[3] The growing demand for LIBs with higher capacity, faster charge–discharge rates, and lower cost underscores the need for new battery materials, architectures, and fabrication methods.[4–9] For example, high capacity anodes based on silicon[10] have been studied extensively, yet challenges remain in controlling their pronounced volumetric changes during lithiation/delithiation cycles. More recently, 3D battery architectures templated from colloidal crystals or holographically defined polymer lattices have been reported that exhibit high charge/discharge rates.[5,11] However, their energy capacity is limited by both the interconnected porosity required for electrolysis deposition as well as the relatively thin conformal electrodes deposited onto these 3D structured current collectors.

A promising alternative approach is to create 3D LIBs with thicker electrodes (≫100 μm).[8,12–15] The volumetric ratio of active/inactive materials within LIBs, and, hence their energy capacity, scales linearly with electrode thickness for a given areal footprint. However, ionic and electronic transport through thicker electrodes is more difficult, which limits their power density.[16–18] To enhance ion transport, researchers have recently focused on fabricating Li-based cathodes with internal open channels oriented orthogonally to current collector surfaces.[4] Using magnetic-field-induced alignment of anisotropic porogens composed of either magnetic particle-coated polymer rods or particle-stabilized emulsion droplets, sintered $LiCoO_2$ cathodes (310 μm thick) were produced with an impressive areal capacity of ≈12 mAh cm^{-2} at a 0.1 C rate.[4] To enhance electronic transport, highly porous metal foams have also been employed as 3D current collectors to create high-performance $LiFePO_4$ (LFP) cathodes (540 μm thick) with an areal capacity of 8.8 mAh cm^{-2} at a current density of 1 mA cm^{-2}.[8] However, the use of thick electrodes also leads to additional challenges, including migration, cracking, and delamination during drying[19] and incomplete electrolyte infiltration.[20]

We recently demonstrated the fabrication of LIBs microbatteries by direct writing of cathode, LFP, and anode, $Li_4Ti_5O_{12}$ (LTO), inks.[7] Specifically, high aspect ratio, interdigitated LFP and LTO electrodes were printed with a wall thickness of ≈60 μm and height between ≈200 and 400 μm onto a glass substrate patterned with gold current collectors. These micro-LIBs (total volume < 1 mm^3) delivered an areal capacity of ≈1.5 mAh cm^{-2} when discharged at rates below 5C. However, due to electronic transport limitations, LFP electrodes printed with eight layers (≈200 μm thick) exhibited the same current density as those with 16 layers (≈400 μm thick). Moreover, it was difficult to hermetically package these micro-LIBs after printing and densification.

Here, we report the design, fabrication, and electrochemical performance of fully 3D printed LIBs composed of thick, biphasic semisolid electrodes that exhibit a ten-fold enhancement in areal capacity compared with our original micro-LIBs. Specifically,[21] these biphasic electrodes consist of well dispersed, active electrode particles (LFP or LTO) mixed with attractive conductive carbon particles that form a percolative network within a lithium-based electrolyte solution. We chose the LFP/LTO electrochemical couple due to its low volumetric change upon cycling[22,23] and exceptional thermal stability,[24,25] which are especially important for fabricating thick electrodes.[16] While Ketjenblack (KB) carbon particles are incorporated as a

Dr. T.-S. Wei, Dr. B. Y. Ahn, J. Grotto, Prof. J. A. Lewis
John A. Paulson School of Engineering and Applied Sciences
Wyss Institute for Biologically Inspired Engineering
Harvard University
Cambridge, MA 02138, USA
E-mail: jalewis@seas.harvard.edu

The ORCID identification number(s) for the author(s) of this article can be found under https://doi.org/10.1002/adma.201703027.

DOI: 10.1002/adma.201703027

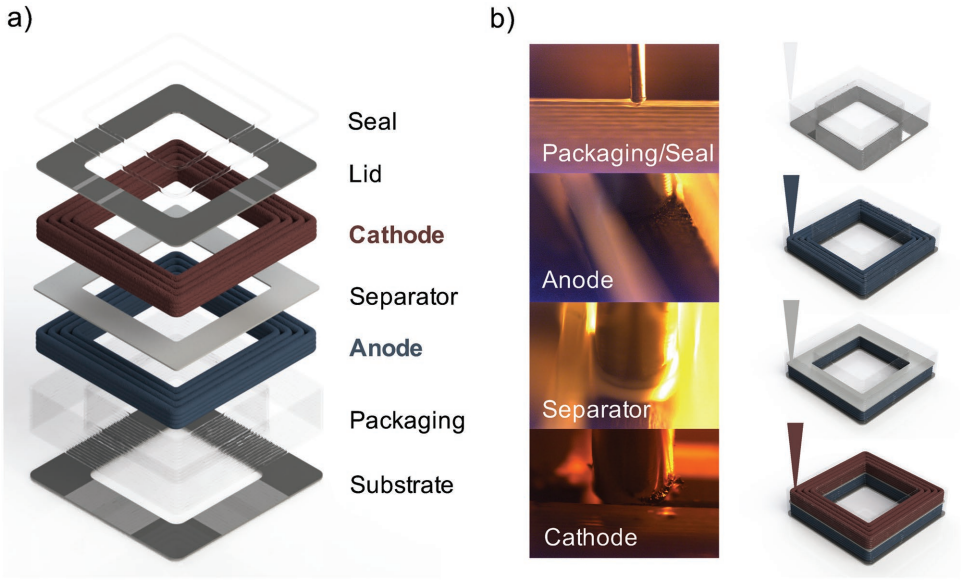

Figure 1. a) Schematic representation (expanded view) of fully 3D printed Li-ion square cell battery with outer dimensions of 1 cm × 1 cm × 2.5 mm and inner hole dimensions of 6 mm × 6 mm. b) Images (left) and schematics (right) of direct writing of four functional (cathode, separator, anode, and packaging) inks.

second phase due to their high electronic conductivity and low percolation threshold.[26] By controlling the respective concentrations and interactions between these two particle populations, we optimized their rheological printing and electronic/ionic transport behavior. We also produced packaging and separator inks composed of ceramic-filled polymer composites that can be UV cured upon direct ink writing. Together, these four inks are used to create fully 3D printed LIBs with thick electrodes patterned in arbitrary geometries (**Figure 1**) encased between two glassy carbon current collectors. Importantly, our additive manufacturing eliminates the need for drying, electrolyte-infilling, calendering, clamping, and heat-sealing processes typically associated with conventional LIB manufacturing.

To create biphasic electrode inks, both the active electrode (LFP or LTO) and conductive KB carbon particle populations are suspended and mixed sequentially in a 1 M lithium bis(trifluoromethane) sulfonamide (LiTFSI)/propylene carbonate (PC) solution. In the absence of a dispersant, each particle population rapidly flocculates due to their inherent van der Waals attraction under high ionic strength conditions.[27] To selectively stabilize the active particles within the concentrated (30 vol%) electrode inks, we added a nonionic dispersant, poly(vinylpyrrolidone) (PVP), at a concentration of 1 wt% with respect to the LFP (or LTO) content. Under these conditions, the PVP-coated LFP and LTO particles are stabilized even at high (1 M) salt concentrations, whereas the KB carbon particles undergo rapid flocculation to produce a percolating conductive network.[28–31]

To optimize their performance, biphasic electrode inks must contain a high active material content coupled with an adequate KB carbon network to overcome the resistive nature of most electrochemically active Li-ion compounds. These electrode inks must also be tailored to exhibit the viscoelastic response required for direct ink writing. Their measured flow curves and shear elastic and loss moduli are shown in **Figure 2**a,b. These electrode inks are strongly shear thinning, which facilitates their flow through fine deposition nozzles. At a characteristic shear rate of 1 s^{-1} associated with printing, the apparent viscosities for LFP and LTO are 6.27 and 1.75 kPa s, respectively. Both electrode inks are elastic-like solids ($G' >> G''$) with respective G' values of 1.59 and 1.25 MPa that flow when their respective shear yield stress (τ_y) values of 3.96 and 1.33 kPa are exceeded. Once these inks exit the nozzle and return to a zero-shear condition, they rapidly solidify and retain their filamentary shape.

Next, we explored the influence of active material content on the electrical conductivity and microstructure of these biphasic electrode inks. To facilitate imaging, we created a model biphasic ink with varying volume fraction of repulsive silica particles, ϕ_{rep} of 0–0.3, at a fixed volume fraction of attractive conductive carbon particles, ϕ_{att} of 0.015. We find that their electronic conductivity increases with increasing ϕ_{rep} (Figure 2c), which results from the observed microstructural evolution within these biphasic inks over the same compositional range (Figure 2d). Notably, the presence of repulsive particles alters the structure of the attractive carbon particle network. In the absence of repulsive particles, the attractive network consists of large, dense clusters surrounded by open regions filled with electrolyte. Upon adding repulsive particles, the attractive carbon particle network becomes more homogenous, favoring the formation of more tenuous chain-like network with fewer bonds between carbon particles. Essentially, the presence of repulsive particles at high volume fractions frustrates the formation of attractive particle bonds thereby yielding aggregated systems that are kinetically trapped in a more structurally uniform state, and hence exhibit a higher electrical conductivity.[32–34]

To fabricate fully 3D printed LIBs, we also produced UV-curable composite inks that serve as packaging and separator materials.[35] Both inks are tailored to exhibit the desired shear thinning and viscoelastic responses required for direct ink writing (Figure 2a,b). The packaging ink is a composite of

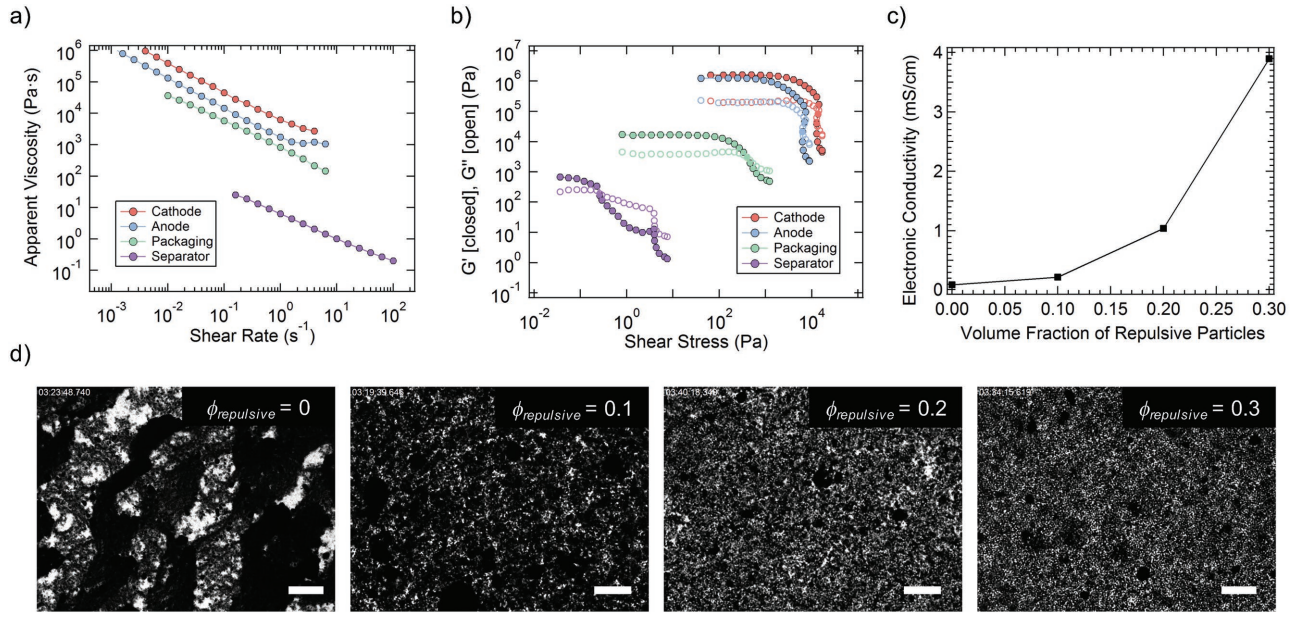

Figure 2. a) Apparent viscosity as a function of shear rate and b) elastic (G') and loss (G'') moduli of the four functional (cathode, separator, anode, and packaging) inks. c) Electronic conductivity as a function of repulsive particle content, and d) optical microscopy images of biphasic mixtures of PVP-stabilized SiO_2 particles and attractive KB carbon particle (1.5 vol% in water–glycerol solution) suspended in an index-matched solution as a function of increasing repulsive particle content (0–30 vol%) [scale bars: 20 μm].

UV-curable epoxy and fumed SiO_2 (4 vol%), which must bond to the current collector and itself during the printing process. After UV curing, it must provide a protective shield to the active electrodes within the printed LIBs. The separator ink is composed of UV-curable ethoxylated trimethylolpropane triacrylate (ETPTA), Al_2O_3 particles, electrolyte (1 M LiTFSI/PC), and photoinitiator.[35] The Al_2O_3 nanoparticles are dispersed using a nonionic dispersant, Triton X-100 (TX-100). Since a thin separator layer is desired, this ink is tailored to have an apparent viscosity and shear elastic modulus that is several orders of magnitude lower than the electrode inks, which facilitates ink wetting and spreading during the printing process.

To investigate the effect of electrode thickness, we carried out AC impedance measurements on LFP/LTO Swagelok cells with thin (0.1 mm) and thick (1 mm) electrodes. As expected, the bulk and charge transfer resistances are higher for thicker electrodes (**Figure 3**a).[8] At low frequencies, these thick electrodes also exhibit a smaller slope due to diffusion-limited transport. Based on DC ohmic measurements, the LFP and LTO electrodes exhibit an electronic conductivity of 13 and 12 mS cm^{-1}, respectively (Figure S1, Supporting Information), which is more than two-fold higher[36] than the ionic conductivity of the electrolyte (5 mS cm^{-1} for 1 M LiTFSI/PC).[37] Cyclic voltammetry measurements reveal that these thick electrodes exhibit a ten-fold higher peak current at low scan rates, albeit with broader redox peaks and peak-to-peak potential-differences, owing to slower kinetics (Figure 3b,c).[38] Moreover, both thin and thick electrodes exhibit excellent Coulombic efficiencies and satisfactory areal capacities over several months of continuous cycling (Figure 3d,e; Figure S2, Supporting Information). While the thick electrodes delivered more than an order of magnitude higher areal capacity compared to their thin counterparts, their energy efficiency falls off considerably with increasing cycle number likely due to increased voltage polarization. Hence, LIBs with thick electrodes are ideally suited for applications that require a high amount of energy, yet fewer charge/discharge cycles. We also measured their self-discharge characteristics, which are important for low power, intermittent applications of interest. The open-circuit voltage for a full LFP/LTO cell with 1 mm electrodes was compared to the discharge curve for an identical cell at 0.2 mA cm^{-2} (Figure 3f). After 20 d, we observed a 0.9% drop in capacity due to self-discharge (Figure S3, Supporting Information), from which we estimate a shelf life of roughly 6 years prior to 100% capacity loss.

Next, we carried out galvanostatic cycling tests with Swagelok cells using standardized stainless steel current collectors with thin Celgard separator films (25 μm) to assess the impact of electrode thickness ranging from 50 μm (i.e., commercial LIBs[12]) to 1 mm (thick LIBs) on cycling performance at current densities varying from 0.2 to 2.0 mA cm^{-2}. **Figure 4**a shows the expected trend of increasing areal capacity with increasing electrode thickness at 0.2 mA cm^{-2}, with 1 mm cells (LFP loading of 108 mg cm^{-2}) delivering ≈14.5 mAh cm^{-2} and a specific capacity of 133 mAh g^{-1}. The Ragone plot (Figure 4b) summarizes the full cycling data (Figure S4, Supporting Information) obtained over a broad range of electrode thicknesses and current densities, which clearly shows that full LFP/LTO cells composed of ultrathick electrodes exhibit superior areal energy density, while largely retaining the areal power density of thin electrodes. The high-rate performance of LIBs with thick electrodes is notoriously poor due to hindered ion diffusion and accelerated local depletion of Li ions at the electrolyte-active particle interfaces.[8,17] However, independent of electrode thickness, we find that the normalized capacity ($Q_{discharge}/Q_{theoretical}$) as a function of current density exhibits nearly the same trend (Figure S5a, Supporting Information). We

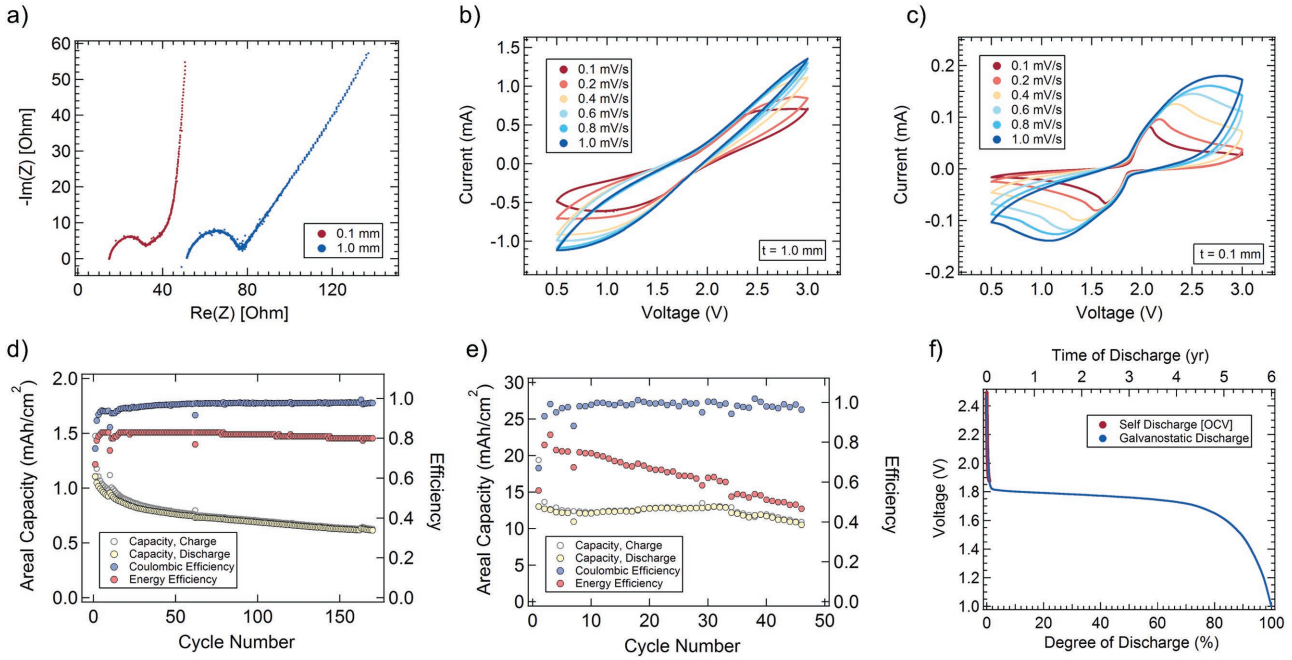

Figure 3. a) AC impedance measurements comparing LFP/LTO Swagelok cells with 0.1 and 1 mm thick electrodes. Cyclic voltammetry data for cells with: b) thick (1.0 mm) and c) thin (0.1 mm) electrodes at scan rates from 0.1 to 1.0 mV s^{-1}. Cycle life at 0.2 mA cm^{-2} for LFP/LTO Swagelok cells with: d) thin (0.1 mm) and e) thick (1 mm) electrodes. f) Self-discharge data measured over 20 d for a LFP/LTO Swagelok cell with thick electrodes. [Note: The galvanostatic discharge curve is plotted alongside this data for a 1 mm thick LFP/LTO Swagelok cell discharged at 0.2 mA cm^{-2}.]

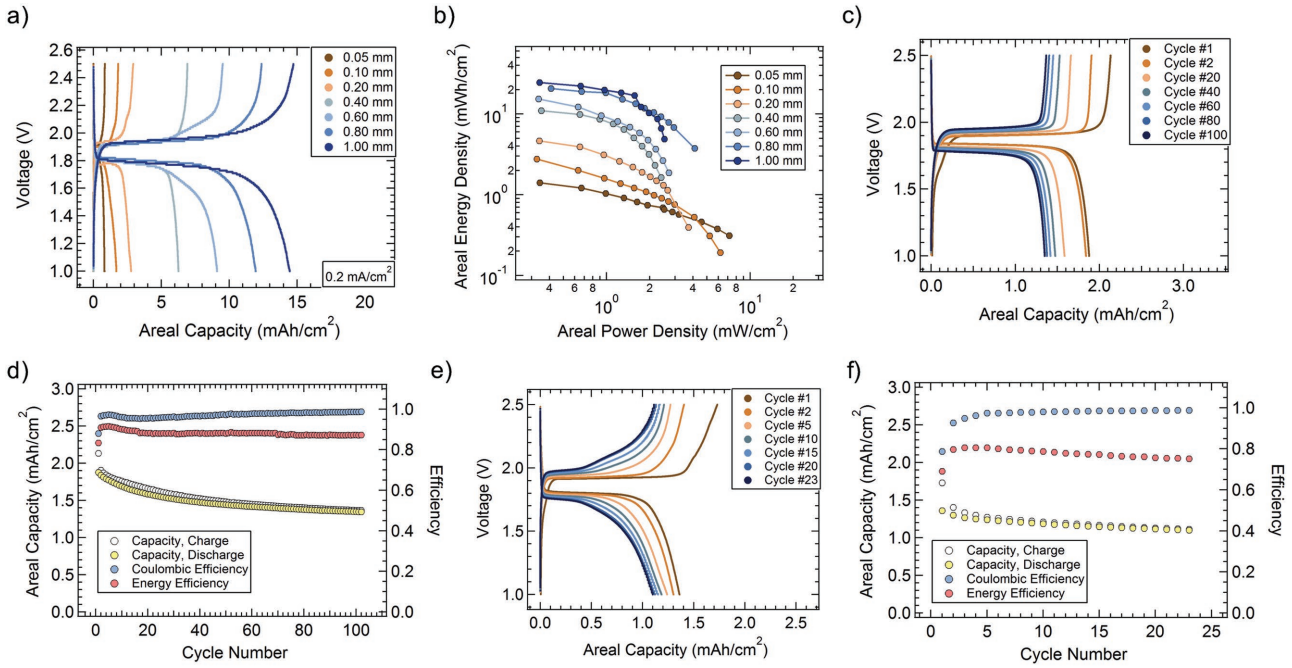

Figure 4. a) Voltage as a function of areal capacity data for LFP/LTO Swagelok cells of varying electrode thickness at 0.2 mA cm^{-2}. b) Ragone plot showing area energy density as a function of areal power density for LFP/LTO Swagelok cells of varying electrode thickness. c) Voltage as a function of areal capacity for varying cycle numbers, and d) areal capacity and Coulombic efficiency as a function of cycle number for a LFP/LTO Swagelok cell with a commercial (Celgard) separator and glassy carbon current collectors and 0.1 mm electrodes cycled at 0.2 mA cm^{-2}. e) Voltage as a function of areal capacity for varying cycle numbers, and f) areal capacity and Coulombic efficiency as a function of cycle number for a LFP/LTO Swagelok cell with printed and UV cured separator and glassy carbon current collectors and 0.1 mm electrodes cycled at 0.2 mA cm^{-2}.

attribute this observation to the efficient distribution of active and conductive particles within these biphasic electrodes[39–41] as well as their high electrolyte content.[12,17,42] From the cycling data, electrodes of varying thickness exhibit a Coulombic efficiency of near unity (Figure S5b, Supporting Information). The observed energy loss (Figure S4c, Supporting Information) is primarily due to the increased overpotential from chemical polarization and heat generation,[8,18,43] which is not unexpected for ultrathick electrodes given their inherently slower diffusion kinetics and increased bulk resistance.

To further explore their electrochemical performance, we created fully 3D printed and packaged LIB with 1 mm thick electrodes in a customized design. Specifically, square cells are produced with an outer border (L = 10 mm, W = 10 mm, H = 2.5 mm) that surrounds an inner, open region (L = 6 mm, W = 6 mm, H = 2.5 mm) (Figure 1; Figure S6a, Supporting Information). The volumetric and gravimetric electrode contents within these printed LIBs are 54 vol% and 63 wt%, respectively (Figure S6b,c, Supporting Information). They are capped on the top and bottom with current collectors that are laser-cut into the desired geometry from a thin glassy carbon sheet. To our knowledge, this is the first time that glassy carbon is used as current collector for LIBs despite its high electrical (3.5×10^{-3} Ω cm) and thermal (17.5 W m^{-1} k^{-1}) conductivity, lightweight, and low gas permeability.[44] Importantly, these laser-cut glassy carbon current collectors remain flat ensuring uniform contact with the printed electrode inks.

Prior to characterizing the performance of fully printed and packaged LIBs, we collected continuous cycling data for a LFP/LTO Swagelok cell with 0.1 mm electrodes using glassy carbon as the current collectors (Figures 4c,d). This full LFP/LTO cell exhibited excellent cycle life with high Coulombic efficiency. Next, we replaced the commercial Celgard separator with a cast and UV cured a 100 µm film produced from our composite separator ink. The cycling performance of this LFP/LTO Swagelok cell with 100 µm electrodes indicates that satisfactory capacity, Coulombic and energy efficiencies are achieved with minimal capacity fade over 20 cycles. The modest decrease in energy efficiency likely arises due to the increased thickness of our composite separator relative to commercial Celgard separator.

As a final demonstration, we characterized the electrochemical performance of fully 3D printed and packaged LIBs composed of thick LFP/LTO electrodes, customized separator and packaging materials, and glassy carbon current collectors. These LIBs deliver an areal capacity of 4.45 mAh cm^{-2} (2nd cycle) at a current density of 0.14 mA cm^{-2}, with the entire area occupied of the battery properly considered (**Figure 5**a).[45] The Ragone plot shows that our fully 3DP LIBs and 1 mm biphasic LFP/LTO full cell data compare favorably to values previously reported for other lithium-ion cells, including those based on coin, Swagelok, and beaker cells (Figure 5b).[4,7,8,13–15,46–53] Our fully printed and packaged LIB also delivers an impressive areal capacity that exceeds the reported values of several other (unpackaged) batteries though not our own unpackaged full cells. In fact, our fully printed and packaged LIBs exhibit a four-fold increase in performance over our unpackaged interdigitated electrode Li-ion microbattery reported previously.[7] While we can use these 1.8 V batteries under ambient conditions to illuminate a LED light (Figure S7, Supporting Information), further optimization is required to improve their capacity, Coulombic efficiency, and energy efficiency to realize their full potential.

In summary, we have demonstrated a new generation of 3DP LIBs with thick, biphasic electrodes in customized form factors. These rechargeable batteries have areal capacities of 4.45 mAh cm^{-2} at 0.14 mA cm^{-2} (which is equivalent to 17.3 Ah L^{-1}), while corresponding full (unpackaged) cells can deliver 14.5 mAh cm^{-2} at 0.2 mA cm^{-2} (energy density ≈20 mWh cm^{-2} at ≈1 mW cm^{-2}). The ability to fabricate high-performance LIBs in nearly arbitrary form factors opens up new avenues for designing wearable electronics, sensors, and other devices, in which batteries may be directly integrated within printed objects, such as eyeglass frames, watch bands, or rings.

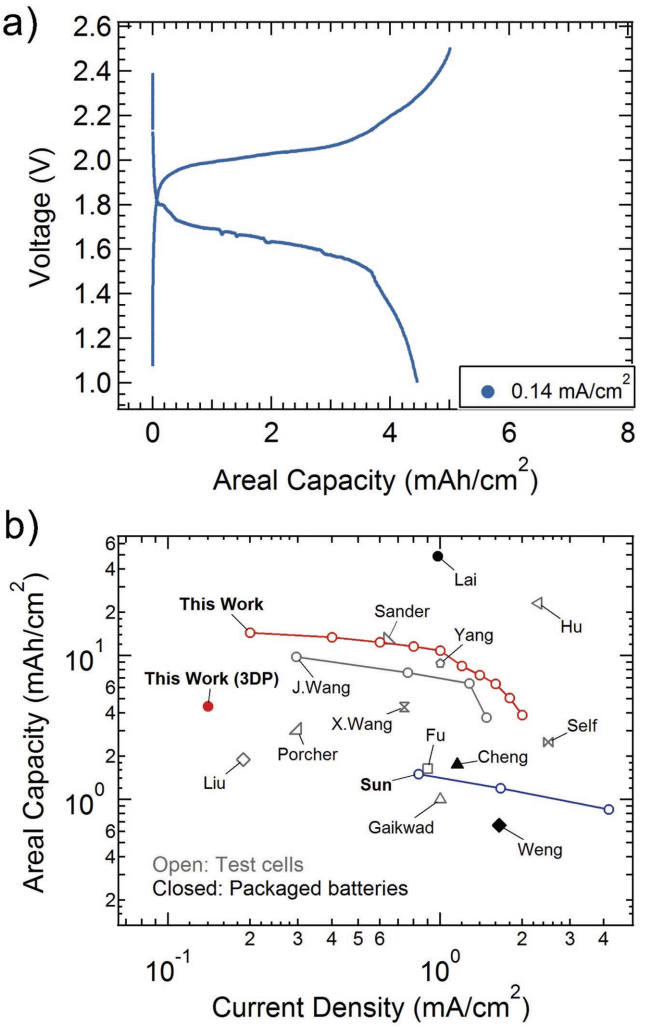

Figure 5. a) Voltage as a function of areal capacity (2nd cycle) at 0.14 mA cm^{-2} for the fully printed and packaged 3DP LIBs composed of ultrathick biphasic LFP and LTO electrodes, UV cured composite separator, UV cured composite packaging, and glassy carbon current collectors. b) Ragone plot comparing areal capacity versus current density for the LFP/LTO Swagelok cell with 1 mm thick electrodes and the fully printed and packaged 3DP LIBs to reported literature values. [Note: Open symbols denote areal capacity values per electrode obtained on test cells; closed symbols denote areal capacity values per battery for fully packaged batteries.]

Experimental Section

Materials and Functional Inks: The materials used to produce the four functional inks included carbon-coated $LiFePO_4$ (M121, Advanced Lithium Electrochemistry Co., Ltd., Taoyuan, Taiwan) and carbon-coated $Li_4Ti_5O_{12}$ (LTO-1, BTR NanoTech Co., Shenzhen, China) active particles, and Ketjenblack (KB) (EC-600JD, Azko Nobel Polymer Chemicals LLC, Chicago, USA) conductive particles. Propylene carbonate (anhydrous, 99.7%), poly(vinylpyrrolidone) (M_w = 40 kg mol^{-1}), TX-100 (laboratory grade), ETPTA (M_w = 428, trivalent acrylate monomer), HMPP (2-hydroxy-2-methyl-1- phenyl-1-propanon, photoinitiator) were acquired from Sigma-Aldrich. Lithium bis(trifluoromethane)sulfonamide (LiTFSI) was provided by BASF. The Al_2O_3 used in the separator ink was supplied by Sumitomo Chemical (AKP-30), while the fumed SiO_2 used in the packaging ink was supplied by Cabot (CAB-O-SIL TS-720). The UV-curing epoxy was obtained from Electronics Materials Inc. (Optocast 3553-40k).

Biphasic electrode inks were prepared in an argon-filled glovebox with moisture and oxygen content maintained under 0.5 ppm. All materials were heated at 120 °C overnight under vacuum to remove moisture. First, 250 mL HDPE bottles were filled with 5 mm (250 g) and 0.5 mm (150 g) yttrium stabilized zirconia milling beads. Next, PC (50 g), PVP (0.1 g), and LFP or LTO powder (10 g) were added. The bottles were sealed and the suspensions were ball-milled (US Stoneware) under ambient conditions for 24 h. The suspensions were then filtered through 20 µm stainless steel sieves in the argon-filled glovebox. The filtered suspensions were sealed in the glovebox and centrifuged (Beckman Avanti J-25 I) at 12 500 g for 30 min to collect the dispersed particles. After removing the supernatant, the dense sediment (typically 65 wt% solids content) was collected and homogenized using a planetary mixer (Thinky AR-100). Additional PC was next added and mixed. LiTFSI was then added to achieve 1 M electrolyte concentration. Finally, KB powder was added and homogenized. The final ink compositions were 30 vol% LFP with 1.25 vol% KB and 30 vol% LTO with 1.35 vol% KB in 1 M LiTFSI/PC with 1 wt% PVP% (with respect to LFP or LTO) for the cathode and anode, respectively.

The separator ink was prepared by ball milling, filtering, and centrifuging an Al_2O_3 suspension the same way as with the biphasic electrode suspensions, but the starting materials were PC (50 g), TX-100 (1 g), and Al_2O_3 powder (20 g) instead. Once the dense sediment (typically 78 wt% solids) was collected in a UV-protected scintillation vial and homogenized, appropriate amount of 2% HMMP solution (ETPTA:HMMP = 100:1) and 1 M LiTFSI/PC were then added and Thinky-mixed. Finally, the ETPTA was added, in which the vial was sealed and vortex-mixed for 30 min at 1500 rpm followed by Thinky-mixing for 1 min to avoid partial curing from overheating. The packaging ink was prepared by mixing 4 vol% of fumed SiO_2 into UV-curing epoxy through multiple cycles of Thinky-homogenization in a UV-protected scintillation vial.

Rheology and Microscopy Characterization: Rheological measurements were performed at 22 °C using an AR-2000EX rheometer (TA Instruments) equipped with stainless steel parallel plates or cone and plate geometries with the appropriate diameter (20, 40, or 60 mm) and gap heights (0.5–1.5 mm). Small diameter parallel plates and larger gap heights were used for high viscosity samples to minimize wall-slip effects. Solvent trap was used to not only prevent evaporation, but also to block UV-light when measuring the separator and packaging inks. Oscillatory measurements (G', G'') were carried out at a fixed frequency (10 rad s^{-1}). All samples were presheared at 1 s^{-1} for 60 s prior to measurement and left to equilibrate until the normal force relaxes (≈60 s). Optical microscopy images of model biphasic mixtures composed of repulsive SiO_2 dispersed with PVP and attractive KB particles suspended in an index-matched water-glycerol solution were taken with an inverted optical microscope (OLYMPUS IX71).

Electrochemical and Conductivity Characterization: All electrochemical experiments were performed using the Biologic VMP-3 potentiostat. A standard galvanostatic cycling setup included a two-electrode Swagelok cell[21] with a porous polymer separator film (Celgard) soaked in electrolyte (1 M LiTFSI/PC), stainless steel current collectors, and PTFE spacers to define the electrode thickness (area = 0.5 cm^2). Glassy carbon and composite separator characterization were performed with circular cutout of them placed appropriately to replace the Celgard separator or stainless steel current collectors. Electronic conductivities of the biphasic electrode inks were measured by the DC method, where the voltage was swept from 0 to 100 mV (Biologic VMP-3). The test cell used was a modified Swagelok cell with a cylindrical volume for the material of interest, sandwiched by two stainless steel electrodes.[21] AC Impedance measurements were carried out using fully assembled Swagelok cells at amplitude of 10 mV and frequency range of 0.1 Hz to 0.3 MHz for the 1.0 mm electrodes, and 1 Hz to 0.2 MHz for the 0.1 mm electrodes. Cyclic voltammetry was also performed using these cells, which were cycled from 0.5 to 3.0 V at various scan rates. Finally, a self-discharge measurement was carried out by first fully charging the battery to 2.5 V at 0.2 mA cm^{-2}, then holding it at 2.5 V for 24 h, then recording the open circuit voltage (OCV) over 20 d.

3D Printed LIBs: 3DP LIBs were fabricated using a custom-made 3D printer that was assembled and operated inside an Ar-filled glovebox consisting of a 3-axis micropositioning stage (Sherline 5400) motorized by stepper motors (CNC4PC, CS4EA4-1Rev1), controlled by computer-aided milling software (Mach3). The cathode, anode, separator, and packaging inks were housed in separate 3 mL syringes (UV-protected ones for separator and packaging inks) and attached by Luer-Loks to the appropriately sized (as small as 100 µm) metal tips (EFD Inc.). An Ar-powered fluid dispenser (HP3cc, EFD Inc.) was used to pressurize the barrel up to 700 psi to control the flow rate. To create the 3DP LIBs, the packaging ink was first printed onto the laser-cut (Photonics Industries, DC150H-355) glassy carbon substrate (Goodfellow, Vitreous 1000C, thickness = 0.18 mm) to 2.5 mm tall followed by 60 min of UV-curing (UVL-21, 365 nm, 4 W, by UVP). Next, the anode ink (1 mm thick layer) was printed onto the glassy carbon substrate within the external border formed by packaging walls. The separator ink was then printed onto the anode to form a thin separator film, followed by 30 min of UV curing. The cathode ink was then printed onto the separator layer with a thickness of 1 mm. The glassy carbon lid was then carefully placed on top of the cathode. Lastly, the packaging ink was printed on top of the lid to seal/bond it to the walls composed of UV cured packaging material. A final UV-curing step (30 min) was carried out to complete the battery fabrication. For 3DP LIBs with thick electrodes, the thicknesses of the substrate, anode, separator, cathode, lid, seal, and packaging were 0.18, 1, 0.1, 1, 0.18, 0.1, and 2.4 mm, respectively.

Electrochemical Characterization of 3D Printed LIBs: The fully 3D printed and packaged LIBs were tested by attaching copper leads to the glassy carbon current collectors with conductive silver paste to avoid excessive clamping force with the usual alligator clamps. The cycling tests were performed at a current density of 0.14 mA cm^{-2}, with the entire area occupied of the battery properly considered.

Supporting Information

Supporting Information is available from the Wiley Online Library or from the author.

Acknowledgements

This work was supported as part of the Joint Center for Energy Storage Research, an Energy Innovation Hub funded by the U.S. Department of Energy, Office of Science, Basic Energy Sciences. The authors thank Koseki Kobayashi and Alex Valentine for their experimental assistance. Finally, the authors thank the Bioinspired Robotics platform within the Wyss Institute and the GETTYLAB for their generous support of our research.

Conflict of Interest

J.A.L. has co-founded Voxel8, Inc, which focuses on 3D printing of functional materials.

Keywords

3D printing, batteries, colloidal suspensions, electrochemistry, Li-ion

Received: May 30, 2017
Revised: November 14, 2017
Published online:

[1] G. Crabtree, E. Kócs, L. Trahey, *MRS Bull.* **2015**, *40*, 1067.
[2] B. Nykvist, M. Nilsson, *Nat. Clim. Change* **2015**, *5*, 329.
[3] J. M. Tarascon, M. Armand, *Nature* **2001**, *414*, 359.
[4] J. S. Sander, R. M. Erb, L. Li, A. Gurijala, Y. M. Chiang, *Nat. Energy* **2016**, *1*, 16099.
[5] J. H. Pikul, H. Gang Zhang, J. Cho, P. V. Braun, W. P. King, *Nat. Commun.* **2013**, *4*, 1732.
[6] N. Liu, Z. Lu, J. Zhao, M. T. McDowell, H.-W. Lee, W. Zhao, Y. Cui, *Nat. Nanotechnol.* **2014**, *9*, 187.
[7] K. Sun, T.-S. Wei, B. Y. Ahn, J. Y. Seo, S. J. Dillon, J. A. Lewis, *Adv. Mater.* **2013**, *25*, 4539.
[8] G.-F. Yang, K.-Y. Song, S.-K. Joo, *RSC Adv.* **2015**, *5*, 16702.
[9] F. Shen, W. Luo, J. Dai, Y. Yao, M. Zhu, E. Hitz, Y. Tang, Y. Chen, V. L. Sprenkle, X. Li, L. Hu, *Adv. Energy Mater.* **2016**, *6*, 1600377.
[10] B. Li, S. Li, J. Xu, S. Yang, *Energy Environ. Sci.* **2016**, *9*, 2025.
[11] H. Zhang, X. Yu, P. V. Braun, *Nat. Nanotechnol.* **2011**, *6*, 277.
[12] M. Singh, J. Kaiser, H. Hahn, *J. Electrochem. Soc.* **2015**, *162*, A1196.
[13] W. Porcher, B. Lestriez, S. Jouanneau, D. Guyomard, *J. Electrochem. Soc.* **2009**, *156*, A133.
[14] X. Wang, Y. Fan, R. A. Susantyoko, Q. Xiao, L. Sun, D. He, Q. Zhang, *Nano Energy* **2014**, *5*, 91.
[15] W. Lai, C. K. Erdonmez, T. F. Marinis, C. K. Bjune, N. J. Dudney, F. Xu, R. Wartena, Y.-M. Chiang, *Adv. Mater.* **2010**, *22*, E139.
[16] H. Zheng, J. Li, X. Song, G. Liu, V. S. Battaglia, *Electrochim. Acta* **2012**, *71*, 258.
[17] F. Jiang, P. Peng, *Sci. Rep.* **2016**, *6*, 32639.
[18] R. Zhao, J. Liu, J. Gu, *Appl. Energy* **2015**, *139*, 220.
[19] J. H. Prosser, T. Brugarolas, S. Lee, A. J. Nolte, D. Lee, *Nano Lett.* **2012**, *12*, 5287.
[20] D. Lv, J. Zheng, Q. Li, X. Xie, S. Ferrara, Z. Nie, L. B. Mehdi, N. D. Browning, J.-G. Zhang, G. L. Graff, J. Liu, J. Xiao, *Adv. Energy Mater.* **2015**, *5*, 1402290.
[21] T.-S. Wei, F. Y. Fan, A. Helal, K. C. Smith, G. H. McKinley, Y.-M. Chiang, J. A. Lewis, *Adv. Energy Mater.* **2015**, *5*, 1500535.
[22] X. Zhang, W. Shyy, A. Marie Sastry, *J. Electrochem. Soc.* **2007**, *154*, A910.
[23] F. Ronci, P. Reale, B. Scrosati, S. Panero, V. Rossi Albertini, P. Perfetti, M. di Michiel, J. M. Merino, *J. Phys. Chem. B* **2002**, *106*, 3082.
[24] S.-Y. Chung, J. T. Bloking, Y.-M. Chiang, *Nat. Mater.* **2002**, *1*, 123.
[25] T.-F. Yi, Y. Xie, Y.-R. Zhu, R.-S. Zhu, H. Shen, *J. Power Sources* **2013**, *222*, 448.
[26] M. Youssry, L. Madec, P. Soudan, M. Cerbelaud, D. Guyomard, B. Lestriez, *Phys. Chem. Chem. Phys.* **2013**, *15*, 14476.
[27] J. N. Israelachvili, *Intermolecular and Surface Forces*, Academic Press, San Diego, CA **1992**.
[28] Y. Zhao, S. Wang, C. Zhao, D. Xia, *Rare Met.* **2009**, *28*, 117.
[29] H. Wang, X. Qiao, J. Chen, X. Wang, S. Ding, *Mater. Chem. Phys.* **2005**, *94*, 449.
[30] L. Zhang, Y. Jiang, Y. Ding, M. Povey, D. York, *J. Nanopart. Res.* **2006**, *9*, 479.
[31] J. Zhang, D. Jiang, Q. Lin, *J. Am. Ceram. Soc.* **2005**, *88*, 1054.
[32] A. Mohraz, E. R. Weeks, J. A. Lewis, *Phys. Rev. E* **2008**, *77*, 060403.
[33] S. K. Rhodes, R. H. Lambeth, J. Gonzales, J. S. Moore, J. A. Lewis, *Langmuir* **2009**, *25*, 6787.
[34] K. C. Smith, P. P. Mukherjee, T. S. Fisher, *Phys. Chem. Chem. Phys.* **2012**, *14*, 7040.
[35] S.-H. Kim, K.-H. Choi, S.-J. Cho, E.-H. Kil, S.-Y. Lee, *J. Mater. Chem. A* **2013**, *1*, 4949.
[36] C. Ye, V. V. Tsukruk, *Science* **2015**, *347*, 130.
[37] T. Nishida, K. Nishikawa, Y. Fukunaka, *ECS Trans.* **2008**, *6*, 1.
[38] Z.-A. Zhang, C.-M. Qu, M. Jia, Y.-Q. Lai, J. Li, *J. Cent. South Univ.* **2014**, *21*, 2604.
[39] B. P. N. Nguyen, S. Chazelle, M. Cerbelaud, W. Porcher, B. Lestriez, *J. Power Sources* **2014**, *262*, 112.
[40] Y. Li, S. Meyer, J. Lim, S. C. Lee, W. E. Gent, S. Marchesini, H. Krishnan, T. Tyliszczak, D. Shapiro, A. L. D. Kilcoyne, W. C. Chueh, *Adv. Mater.* **2015**, *27*, 6591.
[41] A. Kraytsberg, Y. Ein-Eli, *Adv. Energy Mater.* **2016**, *6*, 1600655.
[42] M. F. Hasan, C. F. Chen, C. E. Shaffer, P. P. Mukherjee, *J. Electrochem. Soc.* **2015**, *162*, A1382.
[43] M. R. Palacin, A. de Guibert, *Science* **2016**, *351*, 1253292.
[44] S. Yamada, H. Sato, *Nat. Commun.* **1962**, *4812*, 261.
[45] Y. Gogotsi, P. Simon, *Science* **2011**, *334*, 917.
[46] A. M. Gaikwad, B. V. Khau, G. Davies, B. Hertzberg, D. A. Steingart, A. C. Arias, *Adv. Energy Mater.* **2014**, *5*, 1401389.
[47] Q. Cheng, Z. Song, T. Ma, B. B. Smith, R. Tang, H. Yu, H. Jiang, C. K. Chan, *Nano Lett.* **2013**, *13*, 4969.
[48] L. Hu, F. La Mantia, H. Wu, X. Xie, J. McDonough, M. Pasta, Y. Cui, *Adv. Energy Mater.* **2011**, *1*, 1012.
[49] J. S. Wang, P. Liu, E. Sherman, M. Verbrugge, H. Tataria, *J. Power Sources* **2011**, *196*, 8714.
[50] W. Liu, Z. Chen, G. Zhou, Y. Sun, H. R. Lee, C. Liu, H. Yao, Z. Bao, Y. Cui, *Adv. Mater.* **2016**, *28*, 3578.
[51] K. Fu, Y. Wang, C. Yan, Y. Yao, Y. Chen, J. Dai, S. Lacey, Y. Wang, J. Wan, T. Li, Z. Wang, Y. Xu, L. Hu, *Adv. Mater.* **2016**, *28*, 2587.
[52] E. C. Self, R. Wycisk, P. N. Pintauro, *J. Power Sources* **2015**, *282*, 187.
[53] W. Weng, Q. Sun, Y. Zhang, S. He, Q. Wu, J. Deng, X. Fang, G. Guan, J. Ren, H. Peng, *Adv. Mater.* **2015**, *27*, 1363.